J. Anal. Appl. Pyrolysis 66 (2003) 3–27

JOURNAL of ANALYTICAL and APPLIED PYROLYSIS

www.elsevier.com/locate/jaap

Enhancement of 1,2-dehydration of alcohols by alkali cations and protons: a model for dehydration of carbohydrates

Mark R. Nimlos [a,b,*], Stephen J. Blanksby [b], G. Barney Ellison [b], Robert J. Evans [a]

[a] *National Renewable Energy Laboratory, Golden, CO 80401, USA*
[b] *Department of Chemistry, University of Colorado, Boulder, CO 80309, USA*

Received 5 November 2001; accepted 13 March 2002

Abstract

We have used electronic structure calculations to investigate the 1,2-dehydration of alcohols as a model for water loss during the pyrolysis of carbohydrates found in biomass. Reaction enthalpies and energy barriers have been calculated for neat alcohols, protonated alcohols and alcohols complexed to alkali metal ions (Li^+ and Na^+). We have estimated pre-exponential A factors in order to obtain gas phase rate constants. For neat alcohols, the barrier to 1,2-dehydration is about 67 kcal mol^{-1}, which is consistent with the limited experimental data. Protonation and metal complexation significantly reduce this activation barrier and thus, facilitate more rapid reaction. With the addition of alkali metals, the rate of dehydration can increase by a factor of 10^8 while addition of a proton can lead to an increase of a factor of 10^{23}.
© 2002 Elsevier Science B.V. All rights reserved.

Keywords: 1,2-Dehydration of alcohols; Alkali cations and protons; Dehydration of carbohydrates

---

1. Introduction

The dehydration of carbohydrates is an important process in the pyrolysis of biomass, though the mechanisms and kinetics of this process are not well understood. Loss of water from cellulose can lead to reactive functionalities that can then

---

* Corresponding author
E-mail address: nimlosm@tcplink.nrel.gov (M.R. Nimlos).

0165-2370/02/$ - see front matter © 2002 Elsevier Science B.V. All rights reserved.
PII: S0165-2370(02)00103-1

cross-link, eventually leading to the formation of char, a more highly carbonaceous material that has a higher thermal stability than the original carbohydrate. Dehydration becomes an important consideration in biomass pyrolysis because char formation may be desirable or undesirable. Char pyrolysis is thought to be an important source of polynuclear aromatic hydrocarbons (PAHs), and releases of these toxins in high temperature processes are of concern. On the other hand, dehydration is important in the energy densificaiton of biomass. Slow roasting of biomass at temperature under 300 °C (torrefaction) is known to remove water from biomass and to increase the energy content (per gm) and the density [1,2]. This helps make biomass a better fuel in biomass powered plants and in co-firing with coal. Dehydration during torrefaction is likely due to loss of chemical water contained in carbohydrates. In either case, a more fundamental understanding of dehydration is desirable to optimize or reduce char formation.

In spite of the importance of dehydration of carbohydrates, little mechanistic or kinetic information is available concerning these important reactions. The carbohydrates in biomass contain glycol groups that exist, either on a cyclic or open carbohydrate. For instance, D-glucose has the following cyclic and open forms:

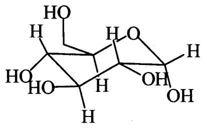

α-pyranose form

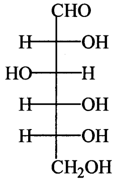

open form

As these structures show, there are numerous adjacent alcohol groups (glycol-like groups). These groups can loose a water through a four-centered transition state involving a hydroxyl group and a hydrogen atom from neighboring carbon atom.

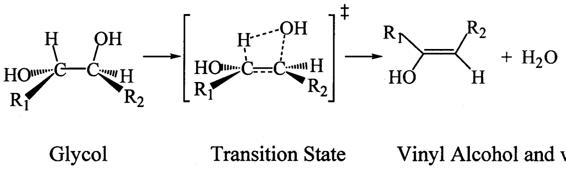

(1)

There are few experimental measurements of these types of reactions, though similar dehydration reactions have been measured for water loss from *tert*-butyl alcohol [4] and 2,3-dimethyl-2-butanol [5].

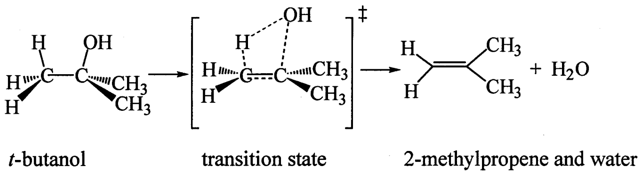

(2)

The temperature dependent rate constants, $k(T)$, for the dehydration of these compounds have been measured and activation energies have been extracted from the Arrhenius equation.

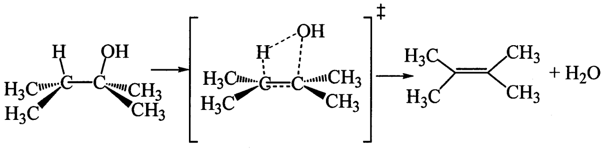
(3)

2,3-dimethylbutan-2-ol transition state 2,3-dimethylbut-2-ene and water

$$k(T) = A \exp\left(-\frac{E_a}{RT}\right) \tag{4}$$

where A is the pre-exponential factor and E_a is the activation energy. These studies have derived activation energies of 66.2 and 64.7 kcal mol^{-1} for reactions (2) and (3).

Some synthetic organic transformations suggest that this relatively high barrier to water loss may be lowered by the addition of alkali metal ions or protons. This may explain some of the phenomena observed with cellulose pyrolysis. For example, it has been demonstrated that the addition of alkali or acid to cellulose enhances the loss of water and the formation of char during pyrolysis [3,9,10]. It may be that these species lower the activation barrier for dehydration reactions such as that shown in (1), which lead to greater unsaturation and thus cross-linking and char formation. For the reaction shown in (1), the barrier to dehydration may be lowered by the complexation of the alkali metal ion or proton to the hydroxy group.

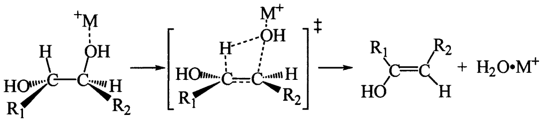
(5)

However, once again, there is little experimental work to rely on to estimate the kinetics for these types of reactions.

In the absence of comprehensive experimental work, we have conducted a molecular modeling study of the dehydration of model compounds to investigate reactions such as (1) and (5). We use *ab initio* electronic structure calculations to determine the structures and energetics of reactants, products and transition states for these important reaction pathways. In addition to molecular geometries and relative energies, we also obtain vibrational frequencies. These molecular parameters are used in statistical mechanics calculations to estimate the rate constants and quantify increases in the rate of dehydration upon the addition of alkali metal ions and protons.

2. Computation details

2.1. Theoretical approach

Electronic structure calculations were performed using the GAUSSIAN 98 [11] suite of programs. Two levels of theory were used in this study: (i) The hybrid density functional theory, B3LYP [12,13] was used initially with a triple *zeta* Pople type basis set, 6-311G(d, p). This technique has been shown to have an RMS error of 3.0 kcal mol^{-1} for the G2 molecule set [67], and produces vibrational frequencies with a reported RMS error [7] of 34 cm^{-1} compared with a set of 122 molecules [8]. For molecules with few heavy atoms, B3LYP/6-311G(d, p) does not require significant computational resources and is excellent for locating minima and transition states. However, comparison with known experimental values indicates that B3LYP often predicts transition state energies lower than the experimental values [18–32] by up to 5 kcal mol^{-1}: (ii) Therefore, we use a Complete Basis Set extrapolation method [14], CBS-QB3, to obtain more accurate transition state energies. This technique uses molecular geometries and frequencies obtained at the B3LYP/6-311G(d, p) level and extrapolates the energy to the complete basis set limit for a CCSD(T) calculation. As a result, this method requires considerably more computational time and memory. CBS-QB3 has a reported RMS error of 2.1 kcal mol^{-1} as determined by comparison to molecules in the G2 set [14]. We will show that this technique is equally accurate for predicting transition state energies.

Since the size of some of the molecules in this study, significant computational resources were required, even for the B3LYP calculations. We used an HP Convex and an SGI super cluster, which were available at the National Center for Supercomputer Applications (NCSA).

2.2. Reaction energies

In our study, we locate molecular geometries of the reactants, transition states and products by finding stationary points on the calculated potential energy surface. A subsequent calculation of vibrational frequencies, obtained from second derivatives of the potential energy, helps ascertain the validity of the optimized geometries. Reactants and products will have all positive vibrational frequencies while transition states will have exactly one negative (imaginary) vibrational frequency, which corresponds to the reaction coordinate. The validity of the transition states is checked with two techniques. We visually inspect the atomic motions of the negative frequency to ensure that they correspond to the reaction coordinate and we conduct Intrinsic Reaction Coordinate [15,16] (IRC) calculations to determine if the transition state connects to the desired products and reactants on the potential energy surface.

Whenever possible, we test the validity of our computational results and the accuracy of the techniques used by comparison to experimental values. As an example, consider the dehydration of *t*-butanol and 2,3-dimethylbutan-2-ol, reactions (2) and (3). We optimized the structure of the reactants and products and obtained energies and enthalpies for these species. From our calculations we obtain the relative enthalpies between the reactants and the products or the enthalpy of reaction $\Delta_{\mathrm{react}}H_{298}$. Our calculated reaction enthalpies for reaction (2) and (3) are shown in Table 1, which also lists the experimental values for these reactions. As can be seen both B3LYP/6-311G(d, p) and CBS-QB3 produce reaction enthalpies that agree to within 3 kcal mol^{-1} of established thermodynamic values.

2.3. Activation energies

The search for transition states for reactions (2) and (3) was started using the geometry of transition state found for the dehydration of ethanol (see below). The arrangement of the atoms involved in the dehydration was similar in the transition states for reactions (2) and (3) as those in the dehydration of ethanol. Starting with the geometry of the transition state for ethanol saved a significant amount of computational time. We located the transition states using either Berny optimization [33] or an eigenvector-following algorithm [34–36]. A comparison of the important bond angles and lengths for the transition states obtained in this study are shown in Table 2. This table also shows the dihedral angle that is related to the out-of-plane angle of the resulting alkene structure. This will be discussed in more detail below.

In order to estimate reaction kinetics, transition state energies are needed, and Table 1 also lists the calculated relative energies at 0 K, ΔE_0, for the transition states of these reactions. The ΔE_0 value contains the zero-point energy as determined from the calculated vibrational frequencies using a scaling factor [14] of 0.99. The Arrhenius activation energy, E_a in Eq. (4), is closely approximated by ΔE_0. As a test of our computational techniques, we compared our calculated ΔE_0 with the experimental E_a values. These are also shown in Table 1 and as can be seen, the CBS-QB3 technique predicts these activation energies within 2 kcal mol^{-1}, but the B3LYP technique underestimates these energies by about 5 kcal mol^{-1}. This is consistent with other calculations of activation energies using B3LYP [18–32] and the accuracy of CBS-QB3 technique is consistent with our earlier study [32].

2.4. Estimates of rate constants

Rate constants for the dehydration of alcohols can be estimated using Transition State Theory (TST). The activation energy for those reactions that have an apparent barrier is approximated by ΔE_0 and the Arrhenius pre-exponential factor in Eq. (4) is approximated by [62]

$$A = \sigma\left(\frac{k_B T}{h}\right)\left(\frac{1}{RT}\right)^{\Delta n}\exp\,(1-\Delta n)\,\exp\left(\frac{\Delta S^{\ddagger}}{R}\right), \tag{6}$$

where σ is the degeneracy (e.g. $\sigma = 3$ for ethanol because of the three equivalent hydrogen), k_B is Boltzmann's constant, h is Plank's constant, R is the gas constant, Δn is the change in number of molecules between the transition state and the

Table 1
Calculated reaction enthalpies, $\Delta_{react}H_{298}$, and relative energies, ΔE_0[a], for transition states

Reaction		B3LYP[b] (kcal mol^{-1})	CBS-QB3 (kcal mol^{-1})	Exptl (kcal mol^{-1})	References
Neat alcohols					
$(CH_3)_3COH \rightarrow$					
$(CH_3)_2CCH_2+H_2O$ ($\Delta_{react}H_{298}$)	**(2)**	13.6	13.7	12.6±0.3	[35]
TS2 (ΔE_0)		59.6	65.9	66.2	[4]
$(CH_3)_2COHCH(CH_3)_2 \rightarrow$					
$(CH_3)_2CC(CH_3)_2+H_2O$ ($\Delta_{react}H_{298}$)	**(3)**	10.8	13.0	10.7±0.4	[39]
TS3 (ΔE_0)		60.4	66.8	64.7	[5]
$CH_3CH_2OH \rightarrow$					
$CH_2CH_2+H_2O$ ($\Delta_{react}H_{298}$)	**(8)**	13.5	11.6	11.0	[40]
TS8 (ΔE_0)		62.7	67.4		
$(CH_3)_2CHOH \rightarrow$					
$CH_2CHCH_3+H_2O$ ($\Delta_{react}H_{298}$)	**(16)**	14.0	13.3	12.2	[43]
TS16 (ΔE_0)		61.5	67.0		
$HOCH_2CH_2OH \rightarrow$					
$CH_2CHOH+H_2O$ ($\Delta_{react}H_{298}$)	**(21)**	8.5	7.9	6.7±2.1	[46]
TS21 (ΔE_0)		63.4	69.6		
Levoglucosan →					
1+H_2O ($\Delta_{react}H_{298}$)	**(25)**	13.4			
TS27 (ΔE_0)		68.3			
Alkali metal complexes					
$CH_3CH_2OH\cdot Li^+ \rightarrow$					
$CH_2CH_2\cdot(H_2O\cdot Li^+)$ ($\Delta_{react}H_{298}$)		8.9	9.9		
$CH_2CH_2+H_2O\cdot Li^+$ ($\Delta_{react}H_{298}$)	**(10)**	17.1	17.5		
TS10 (ΔE_0)		48.2	55.3		
$CH_3CH_2^+ + LiOH$ ($\Delta_{react}H_{298}$)	**(12)**	92.8	94.5		
$CH_3CH_2OH\cdot Na^+ \rightarrow$					
$CH_2CH_2\cdot(H_2O\cdot Na^+)$ ($\Delta_{react}H_{298}$)		8.0	9.7		
$CH_2CH_2+H_2O\cdot Na^+$ ($\Delta_{react}H_{298}$)	**(11)**	15.2	18.1		
TS11 (ΔE_0)		53.1	60.0		
$CH_3CH_2^+ + NaOH$ ($\Delta_{react}H_{298}$)	**(13)**	110.3	114.1		
$(CH_3)_2CHOH\cdot Li^+ \rightarrow$					
$CH_3CHCH_2\cdot(H_2O\cdot Li^+)$ ($\Delta_{react}H_{298}$)		9.3	11.6		
$CH_3CHCH_2+H_2O\cdot Li^+$ ($\Delta_{react}H_{298}$)	**(17)**	19.0	20.8		
TS17 (ΔE_0)		40.4	49.5		
$CH_3CHCH_3^+ + LiOH$ ($\Delta_{react}H_{298}$)	**(18)**	75.3	82.7		
$HOCH_2CH_2OH\cdot Li^+ \rightarrow$					
$CH_2CHOH\cdot(H_2O\cdot Li^+)$ ($\Delta_{react}H_{298}$)		1.3	3.4		
$CH_2CHOH+H_2O\cdot Li^+$ ($\Delta_{react}H_{298}$)	**(22)**	31.9	30.7		
TS22 (ΔE_0)		69.1	74.2		
$CH_3CHOH^+ + LiOH$ ($\Delta_{react}H_{298}$)	**(23)**	72.1	74.5		
Protonated alcohols					
$CH_3CH_2OH_2^+ \rightarrow$					
$CH_2CH_2\cdot H_3O^+$ ($\Delta_{react}H_{298}$)		10.8	12.1		
$CH_2CH_2+H_3O^+$ ($\Delta_{react}H_{298}$)	**(14)**	32.5	32.1	31.6	[49]
TS14(ΔE_0)		18.6	20.7		
$CH_3CH_2^+ +H_2O$ ($\Delta_{react}H_{298}$)	**(15)**	38.5	34.2	33.7	[50]

Table 1 (*Continued*)

Reaction		B3LYP[b] (kcal mol^{-1})	CBS-QB3 (kcal mol^{-1})	Exptl (kcal mol^{-1})	References
$(CH_3)_2CHOH_2^+ \rightarrow$					
$CH_3CHCH_2 \cdot H_3O^+$ ($\Delta_{react}H_{298}$)		10.3	14.0		
$CH_3CHCH_2 + H_3O^+$ ($\Delta_{react}H_{298}$)	**(19)**	37.6	38.1	36.7	[53]
TS19 (?E_0)		7.7	11.8		
$CH_3CHCH_3^+ \cdot H_2O$ ($\Delta_{react}H_{298}$)		7.7	13.5		
$CH_3CHCH_3^+ + H_2O$ ($\Delta_{react}H_{298}$)	**(20)**	24.3	25.1	22.9	[54]
$HOCH_2CH_2OH \cdot H^+ \rightarrow$					
$CH_3CHOH^+ \cdot H_2O$ ($\Delta_{react}H_{298}$)		−13.7	−11.4		
$CH_3CHOH^+ + H_2O$ ($\Delta_{react}H_{298}$)	**(24)**	3.5	1.6	7.0	[56]
TS24		24.4	27.6		

[a] The relative energies for the transition states contain the zero point energy.

[b] Using a 6-311G(d, p) basis set.

reactants (in this case $\Delta n = 0$) and $\Delta S^{\ddagger}$ is the difference in entropy between the transition state and the reactant. We use the entropy obtained from electronic structure calculations using GAUSSIAN 98. The classical approximation is used to obtain entropies form vibrational frequencies and molecular structures using the rigid rotor and harmonic oscillator (HO) approximation. The vibrational frequencies are used without scaling. We have found that scaling the vibrational frequencies changes $\Delta S^{\ddagger}$ by much less than 1 cal mol^{-1} K^{-1} and has little effect upon the A factor.

To properly treat aliphatic alcohols, one must consider the hindered internal rotors when calculating entropies. Calculations with electronic structure techniques usually obtain vibrational frequencies by determining second order derivatives of the potential at a potential minimum. Therefore, the actual potentials for the hindered rotors are greatly oversimplified. These potentials should have relatively low barriers (1–5 kcal mol^{-1}) as a function of rotations about C–C and C–O bonds. Vibrational frequencies obtained from the second derivatives at potential minima will be harmonic frequencies. Using the HO approximation will result in an underestimate of the density of states and the entropy for these molecules.

Since we are only interested in the relative entropy, $\Delta S^{\ddagger}$ in Eq. (6), for calculating rate constants, we can make some simplifications when treating the hindered rotors. For these 1,2-dehydration reactions, there are two rotors that will be greatly changed between the alcohol and the transition state; the rotation about the C–C bond involving the OH group and the rotation about the C–O bond. For ethanol, these are shown below.

Table 2

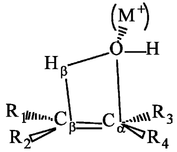

Transition state geometries

Alcohol	M^+	r (O–H_β) (Å)	r (C_β–H_β) (Å)	r (C_β–C_α) (Å)	r (C_α–O) (Å)	α(C_α–O–H_β) (°)	Dihedral R_3–C_α–C_β–R_4 (°)
$(CH_3)_3COH$		1.32	1.34	1.43	2.02	59.3	159.8
$(CH_3)_2COHCH(CH_3)_2$		1.35	1.31	1.44	2.08	57.2	162.9
CH_3CH_2OH		1.26	1.43	1.42	1.86	63.8	140.3
	H^+	1.97	1.18	1.40	2.53	41.5	175.8
	Na+	1.54	1.25	1.40	2.24	48.8	176.1
	Li^+	1.63	1.22	1.40	2.32	46.0	178.9
$(CH_3)_2CHOH$		1.29	1.38	1.42	1.94	61.3	159.4
	H^+	1.99	1.14	1.42	2.84	41.1	177.9
	Li^+	1.71	1.18	1.41	2.51	45.6	178.0
$HOCH_2CH_2OH$		1.25	1.45	1.42	1.87	63.1	156.4
	H^+	2.18	1.17	1.41	2.34	44.6	178.9
	Li^+	1.80	1.22	1.40	2.27	43.7	175.0

From B3LYP/6-311G(d, p) calculations.

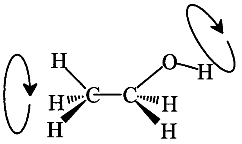
(7)

Hindered rotors for ethanol

The HO approximation for these two modes will underestimate the entropy by about 1 cal mol^{-1} K^{-1} for each internal rotor [68]. This will lower the pre-exponential factor by about a factor of 3. We have used the technique of Ayala *et al.* [38] that is implemented in GAUSSIAN 98 to estimate the contribution of the rotors similar to those in (7) to $\Delta S^{\ddagger}$ and the Arrhenius pre-exponential factor, A. For the molecules considered here, we assume that all other internal rotations are cancelled out when calculating $\Delta S^{\ddagger}$. The A factors calculated with this hindered rotor approximation are shown in Table 3. The A factors obtained for the dehydration of neat 2,3-dimethylbutanol and *t*-butanol (6.6×10^{13} and 1.3×10^{14} s^{-1}) show good agreement with the experimental values (4.57×10^{13} and 3.98×10^{14} s^{-1}).

3. Results and discussion

3.1. Ethanol

Ethanol is the simplest alcohol capable of undergoing a 1,2-dehydration reaction. It will, therefore, serve as a good model system for our investigation. This reaction proceeds through a four-centered transition state and produces ethylene and water.

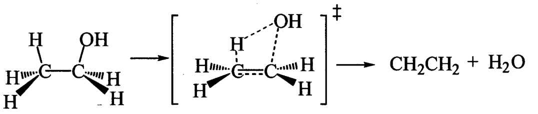
(8)

Ethanol TS8 Ethylene and Water

As discussed above, we obtained stationary points for ethanol, ethylene and water. The calculated enthalpies for these species are used to estimate the ethalpy for reaction (8), $\Delta_{\mathrm{react}}H_{298}$. The values obtained using both B3LYP and CBS-QB3 are listed in Table 1. The CBS-QB3 value is in agreement to better than 1 kcal mol^{-1} with established thermochemistry.

We obtain a transition state (TS8) for reaction (8) using techniques described above and our structure is similar to that obtained earlier using MP2 calculations [6]. Frequency calculations at the transition state produced exactly one negative vibrational frequency, 1948i cm^{-1}. Fig. 1 shows a scaled representation of the transition state and the vectors representing the atomic motion. These vectors are consistent with a concerted a 1,2-dehydration reaction. The atomic motion of the reaction coordinate is similar to that found with MP2 for 1,2-dehdyration in ethanol

Table 3
Rate constants calculated using transition state theory

Reaction		E_a (kcal mol^{-1})^a	A (s^{-1})	k(250 °C) (s^{-1})	k(500 °C) (s^{-1})
$(CH_3)_2COHCH(CH_3)_2 \rightarrow (CH_3)_2CC(CH_3)_2 + H_2O$	(2)	66.8	6.6×10^{13}		
$(CH_3)_3COH \rightarrow (CH_3)_2CCH_2 + H_2O$	(3)	65.9	1.3×10^{14}		
$CH_3CH_2OH \rightarrow CH_2CH_2 + H_2O$	(8)	67.4	2.7×10^{13}	1.8×10^{-15}	2.4×10^{-6}
$CH_3CH_2OH \cdot Li^+ \rightarrow CH_2CH_2 + H_2O \cdot Li^+$	(10)	55.3	4.5×10^{13}	3.5×10^{-10}	1.0×10^{-2}
$CH_3CH_2OH \cdot Na^+ \rightarrow CH_2CH_2 + H_2O \cdot Na^+$	(11)	60.0	6.8×10^{12}	5.6×10^{-13}	7.2×10^{-5}
$CH_3CH_2OH_2^+ \rightarrow CH_2CH_2 + H_3O^+$	(14)	30.7	2.8×10^{14}	4.1×10^{1}	5.8×10^{5}
$CH_3CH_2OH \cdot Li^+ \rightarrow CH_3CH_2^+ + LiOH$	(12)	93.5	10^{16}	8.2×10^{-24}	3.6×10^{-11}
$CH_3CH_2OH \cdot Na^+ \rightarrow CH_3CH_2^+ + NaOH$	(13)	112.9	10^{16}	6.3×10^{-32}	3.9×10^{-16}
$CH_3CH_2OH_2^+ \rightarrow CH_3CH_2^+ + H_2O$	(15)	32.8	10^{16}	2.0×10^{2}	5.4×10^{6}
$(CH_3)_2CHOH \rightarrow CH_3CHCH_2 + H_2O$	(16)	67.0	8.2×10^{13}	8.4×10^{-15}	9.5×10^{-6}
$(CH_3)_2CHOH \cdot Li^+ \rightarrow CH_3CHCH_2 + H_2O \cdot Li^+$	(17)	49.5	2.2×10^{14}	4.6×10^{-7}	2.3×10^{0}
$(CH_3)_2CHOH_2^+ \rightarrow CH_3CHCH_2 + H_3O^+$	(19)	36.9	7.3×10^{14}	2.8×10^{-1}	2.7×10^{4}
$(CH_3)_2CHOH \cdot Li^+ \rightarrow CH_3CHCH_3^+ + LiOH$	(18)	81.5	10^{16}	9.1×10^{-19}	3.4×10^{-8}
$(CH_3)_2CHOH_2^+ \rightarrow CH_3CHCH_3^+ + H_2O$	(20)	22.7	10^{16}	3.4×10^{6}	3.9×10^{9}
$HOCH_2CH_2OH \rightarrow CH_2CHOH + H_2O$	(21)	69.6	1.2×10^{14}	1.0×10^{-15}	2.6×10^{-6}
$HOCH_2CH_2OH \cdot Li^+ \rightarrow CH_2CHOH + H_2O \cdot Li^+$	(22)	74.2	8.5×10^{14}	8.4×10^{-17}	8.9×10^{-7}
$HOCH_2CH_2OH \cdot H^+ \rightarrow CH_3CHOH^+ + H_2O$	(24)	27.6	9.6×10^{14}	2.7×10^{3}	1.5×10^{7}
$HOCH_2CH_2OH \cdot Li^+ \rightarrow CH_3CHOH^+ + LiOH$	(23)	73.2	10^{16}	2.6×10^{-15}	2.0×10^{-5}

[a] Derived from CBS-QB3 calculations. See text.

[6]. This transition state was shown to connect ethanol with ethylene and water using IRC calculations.

The calculated energy of this transition state gives a value for ΔE_0 of 67.4 kcal mol^{-1}. Our computed barrier is consistent with: (i) the MP2 computed values [6] (67 kcal mol^{-1}) and (ii) the experimental barriers for 1,2-dehydration of *t*-butanol and 2,3-butan-2-ol. The high energy of this transition state is also consistent with its calculated structure. Critical bond lengths and angles for the transition state in reaction (8) are collected in Table 2. The long C–O bond length (1.86 Å) suggests that to a significant extent this bond has been broken, thus requiring a significant portion of the C–O bond dissociation enthalpy for ethanol, DH_{298} (CH_3CH_2–

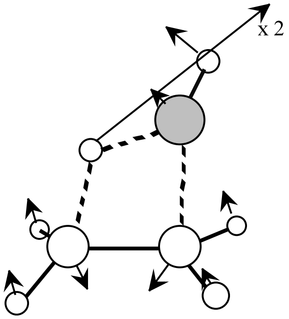

Fig. 1. A scaled drawing of the transition state for 1,2-dehydration of ethanol, TS8, determined by B3LYP/6-311G(d, p) calculations. The arrows show the atomic motions of the reaction coordinate. The long arrow from the reactive H atom has been reduced by 50%.

OH) = 93.9 ± 0.4 kcal mol^{-1}. Some of this energy is offset due to partial bond formation between the H and O atoms.

The other critical bond lengths and angles of the transition state presented in Table 2 provide additional information about the development of the 1,2-dehydration. The HCCH dihedral angle (defined in the table) is about 140°, which is between the dihedral angle in ethanol (118°) and ethylene (180°), and the C–C bond length (1.42 Å) is between the C–C length for ethanol (1.52 Å) and ethylene (1.33 Å). These values show the progress in reaction (8) in converting ethanol to ethylene plus water.

In order to estimate the rate constant for 1,2-dehydration of ethanol, we use (6) to estimate the pre-exponential A factor. We used the hindered rotor calculation available in GAUSSIAN 98 to account for the two internal rotations shown in (7). This amounted to a correction of 0.8 cal mol^{-1} K^{-1} in $\Delta S^{\ddagger}$ and a correction of less than a factor of 2 in the pre-exponential A factor. The calculated A factor for 1,2-dehydration of ethanol (Fig. 3) is 2.7×10^{13} s^{-1} and with the calculate activation energy, $\Delta E_0(\sim E_a) = 67.4$ kcal mol^{-1} we can estimate the rate constant for this process. In Table 3, we present the rate constant at temperatures typical for torrefaction, $k(250\ ^{\circ}\mathrm{C}) = 1.8 \times 10^{-15}$ s^{-1}, and pyrolysis, $k(500\ ^{\circ}\mathrm{C}) = 2.4 \times 10^{-6}$ s^{-1}. These rate constants are small, as would be expected for reaction with such a high activation energy, and this suggests that this type of dehydration is inefficient.

3.2. Stabilization of TS8

The Mulliken charges calculated from the CCSD(T) portion of the CBS calculation for ethanol and the dehydration transition state (TS8) are shown below.

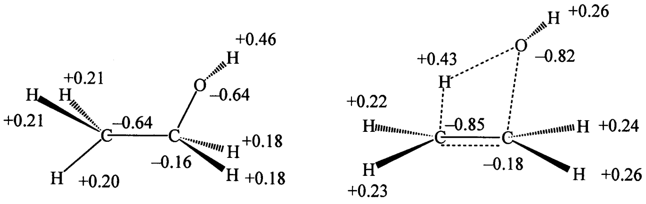

Mulliken charges for ethanol TS8

(9)

As can be seen there is appreciable build up of negative charge on the oxygen atom in the transition state relative to ethanol. Thus, one would expect that the transition state would be stabilized relative to ethanol by complexation with a positive ion. We discuss several examples below.

3.3. Ethanol with alkali metal ions

As mentioned above, addition of alkali metal ions to cellulose has a profound effect upon the pyrolysis of cellulose. We have investigated this by considering the effect of added alkali cations on the reaction energies and barrier heights for 1,2-dehydration. The influence of Li^+ and Na^+ on the 1,2-dehydration of ethanol is shown in Table 1. With both cations the final products are ethylene and the cation complexed to a water molecule. Along the reaction coordinate to forming these products, a complex is formed between the hydrated alkali cation and ethylene. These reactions paths are shown in (10) and (11).

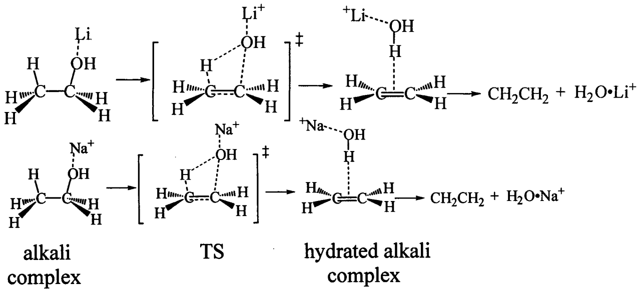

(10)

(11)

The calculated complexation enthalpies for these alkali cations with ethanol and water are shown in Table 4. Since the enthalpy of complexation of the alkali with water is about 6 kcal mol^{-1} smaller than that for ethanol, the enthalpy of reactions (10) and (11) are more endothermic than the dehydration of neat ethanol, reaction (8). The effects of the alkali metal upon the structure of ethanol and water in the complexes is shown in Fig. 2. As can be seen the effect is slight for these alkali cations. This Figure also shows that the bond between the cation and the oxygen atom is significantly shorter (0.38 Å) for Li^+ than for Na^+, which explains the higher binding energy for Li^+.

Table 4
Calculated binding enthalpies, $\Delta_{\text{bind}}H_{298}$, for complexes

Molecule/M$^+$	H^{+a}	Li$^+$	Na$^+$
CH_3CH_2OH	182.9, experimental: 185.6[b]	38.6	26.7
$(CH_3)CHOH$	187.3, experimental: 189.5[b]	40.3	
$HOCH_2CH_2OH$	187.1, experimental: 195.0[b]	58.4	
H_2O	162.6, experimental: 165.0[b]	33.1	20.9

Using CBS-QB3. The binding enthalpy, $\Delta_{\text{bind}}H_{298}$, is defined as the enthalpy for the reaction ROH·M$^+$ × ROH+M$^+$.

[a] Defined as proton affinities.

[b] [17].

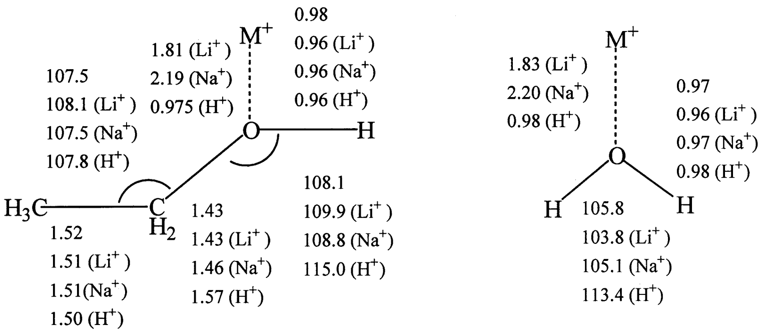

Fig. 2. Critical bond lengths (in Å) and angles (in °) for ethanol and water neat and complexed with M$^+$ = Li$^+$, Na$^+$, and H$^+$, calculated using B3LYP/6-311G(d, p).

In addition to the reactions shown in (10) and (11), the ethanol/alkali complex can also form ethyl cation [63] and hydroxylated alkali metal.

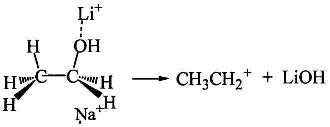

(12)

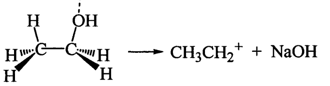

(13)

The calculated enthalpies of these reaction are high ($\Delta_{\text{react}}H_{298} = 94.5$ kcal mol^{-1} for Li$^+$ and 114.1 kcal mol^{-1} for Na$^+$) as is shown in Table 1. We could not locate complexes of the carbocation with the hydroxylated alkali metal.

The effect of these alkali metal cations upon the transition state for 1,2-dehydration is profound. The decrease in the barrier to dehydration is shown graphically in Fig. 3 for ethanol complexed to Li$^+$. For the complex with Li$^+$, the barrier for dehydration is about 12 kcal mol^{-1} lower than for neat ethanol, while for Na$^+$ the barrier is lowered by about 7 kcal mol^{-1}. As discussed above, this trend is

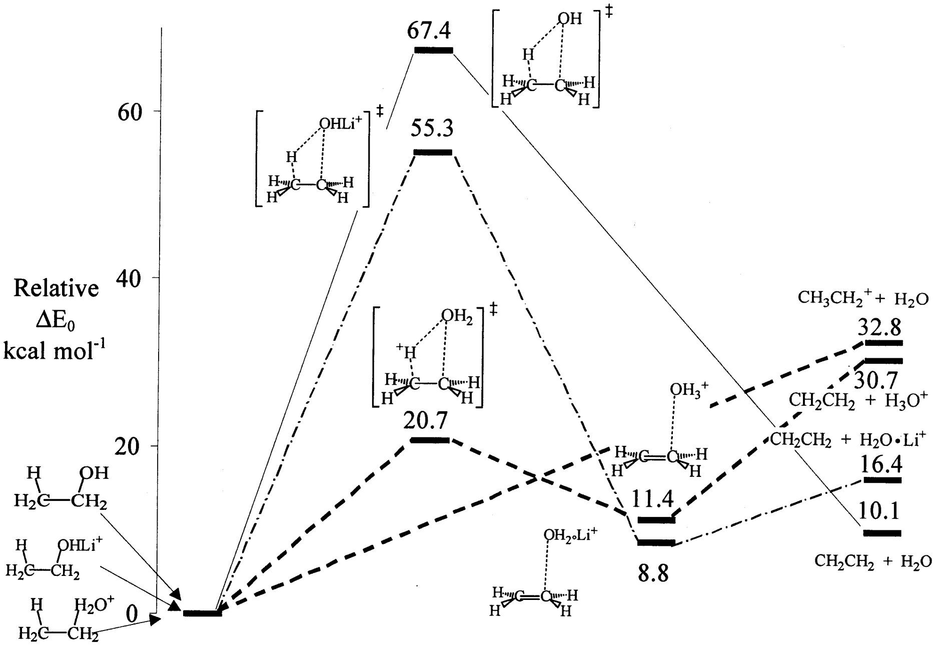

Fig. 3. Schematic diagram of the energetics of the 1,2-dehydration of ethanol. The solid line is for neat ethanol, reaction (8), the dashed–dotted line is for lithiated ethanol, reaction (10), and the dashed line is for protonated ethanol, reactions (14) and (15). The calculated relative energies, ΔE_0, are obtained using CBS-QB3 and include zero point energy.

likely due to the long Na^+–O bond length (2.14 Å) in the transition state relative to the short Li^+–O bond length (1.75 Å). These alkali metal cations also have the expected effect of making the transition state appear more like the products as is shown in Table 2. Note that the dihedral angles (e.g. 179° for Li^+) are now close to the value for ethylene (180°), though to a lesser extent for Na^+ than Li^+. As described above, we have used our calculated activation energies and entropies to calculate rate constants for 1,2-dehydration of the alkali complexes and the results are shown in Table 3. The rate constant increases by roughly 5 orders of magnitude with Li^+ and 2 orders of magnitude for Na^+. For K^+, an important alkali metal in biomass, one can anticipate that the effect will be further diminished, because of its larger size. These increases in the rate constants show that 1,2-dehydration is significantly more efficient with alkali metal cations present.

We also estimated rate constants for reactions (12) and (13) even though we could not locate a transition state. Since this is a simple bond dissociation, we used the energy of these reactions (93.5 and 112.9 kcal mol^{-1}) for E_a and assumed a high pre-exponential A factor (10^{16} s^{-1}), as one would expect for a loose transition state. Even with these large A factors, the rate constants for these reactions are extremely small. They are 9–19 orders of magnitude smaller than the rate constant for reactions (10) and (11), and thus, these channels are likely to be unimportant.

3.4. Protonated ethanol

Protonation of ethanol produces a larger effect upon the dehydration reaction. The 1,2-dehydration reaction in the presence of a proton is shown in reaction (14).

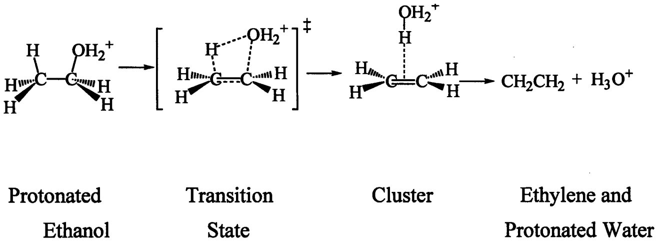

(14)

The proton affinities (defined [17] as the enthalpy of adding a proton at 298 K) for ethanol and water are presented in Table 4. Our calculated proton affinities are compared with literature values in this table and for ethanol and water our calculated values are within 3 kcal mol^{-1} of the experimental values. This discrepancy between the CBS-QB3 results and experimental measurements may be due to the lack of diffuse functions in the basis set used [37]. The difference in proton affinity between water and ethanol is high, 20 kcal mol^{-1}, and as a result reaction (14) is 20 kcal mol^{-1} more endothermic than dehydration of neat ethanol (8). Our calculated reaction energy for (14), 30.7 kcal mol^{-1}, is consistent with a value obtained using [64] MP4/6-311G(d, p)//MP2/6-31G(d), 31.1 kcal mol^{-1}, and our energy for the cluster (11.4 kcal mol^{-1}) is also in agreement with these MP4 calculations (12.7 kcal mol^{-1}).

As can be seen in Fig. 2, the effect of an added proton upon the structures of ethanol and water is also profound. In ethanol the C–O bond is lengthened from 1.43 Å for neat ethanol to 1.57 Å for protonated ethanol. MP4 calculations [64] yielded a similar value, 1.55 Å. This is presumably due to the strong bond formed between the proton and the oxygen atom.

As shown in Fig. 3 and Table 1, protonation of ethanol produces a larger reduction in barrier to dehydration relative to the addition of Li$^+$. The barrier is nearly 47 kcal mol^{-1} lower than for neat ethanol and roughly 30 kcal mol^{-1} lower than dehydration of ethanol facilitated by Li$^+$. Our CBS energy for this transition state, 20.7 kcal mol^{-1}, is comparable to the value obtained with MP4 calculations [64]. The greater energetic stability of the protonated transition state is also reflected in its structure. As described for neat ethanol, the C–O bond is lengthened considerably in the transition state (1.86 Å for the TS compared with 1.43 Å for ethanol) and because the charge separation of the transition state is stabilized by the proton, this effect is enhanced in the protonated transition state. The structure we obtain for the transition state is completely consistent with that obtained using MP4 [64]. The C–O bond length in the TS is now 2.53 Å (2.46 Å using MP4 [64]). The critical dihedral angle in the transition state (177.8°, 117.2 ° using MP4 [64]) is also significantly larger than for neat ethanol (140.3°). This value is closer to that of ethylene (180°) than ethanol (118°), suggesting a late transition state, and consistent with a highly endothermic process.

A consequence of the stabilization of the transition state in reaction (14) is that its energy (20.7 kcal mol^{-1}) is now lower than the energy of the isolated products (30.7 kcal mol^{-1}). As a result, calculating the rate constant for reaction (14) using the energy of the transition state as the activation energy (E_a) will greatly overestimate the rate constant for this reaction. Proper treatment of this reaction requires RRKM analysis. However, for a rough estimate of the rate constant we will simply use the reaction energy as E_a in Eq. (4), and we use the TST, Eq. (6), to calculate the A factor. That is, $\Delta S^{\ddagger}$ will still be calculated using the structure and frequencies of the transition state. The rate constants for this reaction (Table 3) are 11–16 orders of magnitude greater than neat ethanol, making dehydration of protonated ethanol much more efficient. Despite the approximations made in determining these rate constants, the increase in dehydration rate upon protonation of ethanol is quite dramatic. The lifetime of these reactions (the inverse of the rate constants, $\tau_{250\ °C} = 2 \times 10^{-2}$ s, $\tau_{500\ °C} = 2 \times 10^{-6}$ s) is such that these reactions would be complete within the typical residence time of an industrial reactor (e.g. 0.1–1 s).

In addition to loss of H_3O^+, protonated ethanol can undergo a loss of H_2O to form a carbocation.

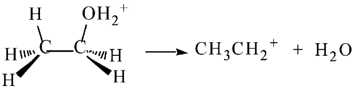

(15)

We conducted potential energy surface calculations, where the C–O bond in protonated ethanol is incrementally lengthened and all other internal coordinates are allowed to adjust to the lowest energy configuration. The energies obtained for these calculations show that there is no barrier for the reverse of reaction (15), which is consistent with what was found using MP4 [64]. We did not find an energetically stable cluster between H_2O and ethyl cation, which is also consistent with this MP4 study [64]. Consistent with established thermochemistry (Table 1), we find that reaction (15) is only 3 kcal mol^{-1} more endothermic than reaction (14). The rate constants that we obtain for reaction (15) are slightly larger than those for reaction (14) due to the loose transition state (large A factor) associated with reaction (15). The rate constants for this reaction are 12–15 orders of magnitude larger than those for dehydration of neat ethanol. The short lifetimes for reaction (15), $\tau_{250\ °C} = 5 \times 10^{-3}$ s, $\tau_{500\ °C} = 2 \times 10^{-7}$ s, are such that this type of reaction could also be important in practical pyrolysis applications. Importantly, this type of reaction forms a carbocation, which is a very reactive species that could be important in cross-linking and char formation.

The relative rate constants that we obtain for reactions (14) and (15) are consistent with collisionally induced dissociation (CID) mass spectrometry experiments of protonated ethanol [65,66]. These experimental studies show that $C_2H_5^+$ ($m/z = 29$) is preferentially formed over H_2O^+ ($m/z = 19$) during collisions of protonated ethanol with a collision gas. This is consistent with our calculations showing that reaction (15) is roughly an order of magnitude larger than reaction (14).

3.5. Isopropanol

Most carbohydrates have OH groups bonded to secondary carbons, and we investigated 1,2-dehydration of isopropanol to identify differences from ethanol, where the OH group is on a primary carbon. With neat isopropanol, 1,2-dehydration yields products analogous to those from ethanol.

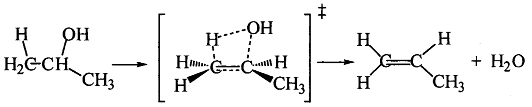

(16)

The enthalpy of this reaction ($\Delta_{\text{react}}H_{298} = 13.3$ kcal mol^{-1}) and the barrier to dehydration ($\Delta E_0 = 67.0$ kcal mol^{-1}) are calculated to be similar to those values for ethanol, Table 1. The transition state structure, Table 2, is also similar to that for ethanol except that the C–O bond (1.94 Å) is longer and the critical dihedral angle (159.4°) is larger, suggesting a later transition state. The Mulliken charge distribution in the transition state shows a greater charge separation than in the transition state for ethanol, due to the ability of the secondary carbon atom to accommodate more positive charge.

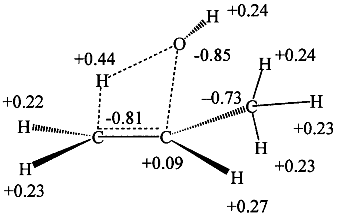

Mulliken charges in transition state

Thus, one would expect a larger influence of added positive ions. The addition of Li$^+$ has a more profound effect upon the barrier for isopropanol than it does for ethanol, lowering the dehydration barrier 17 kcal mol^{-1} for isopropanol compared with 12 kcal mol^{-1} for ethanol. The result of this lowered barrier is a calculated rate constant for reaction (17) that is 6–8 orders of magnitude greater than the rate for neat isopropanol, as shown in Table 3.

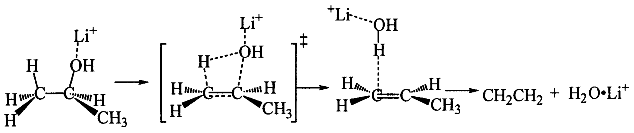

(17)

Due to the greater stability of secondary carbocations relative to primary carbocations, the enthalpy for the reaction (18) is roughly 12 kcal mol^{-1} lower than for ethanol.

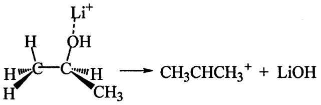

(18)

However, the reaction barrier for (18) is still high, 81.5 kcal mol^{-1}, and the calculated rate constants are still 8–12 orders of magnitude smaller than those for reaction (17). Again, Li$^+$ greatly increases dehydration through the loss of $H_2O \cdot Li^+$, though formation of the carbocation is insignificant.

The effect of greater stability of the carbocation is particularly impressive with protonated isopropanol, as is shown in Table 1 and Fig. 4. Here the formation of propylene, reaction (19) is about 5 kcal mol^{-1} more endothermic than the analogous channel for ethanol.

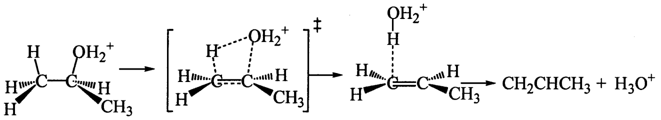

(19)

Conversely, the energy of reaction barrier for this reaction, $\Delta E_0 = 11.8$ kcal mol^{-1}, is significantly lower than the barrier for protonated ethanol, $\Delta E_0 = 20.7$ kcal mol^{-1}. As was the case with ethanol, the transition state is at a lower in energy than the separated products and thus, we use the reaction energy as the activation energy, E_a, instead of the energy of the transition state. The A factor was calculated with TST using the transition state shown in (19). The resulting rate constants are 10–14

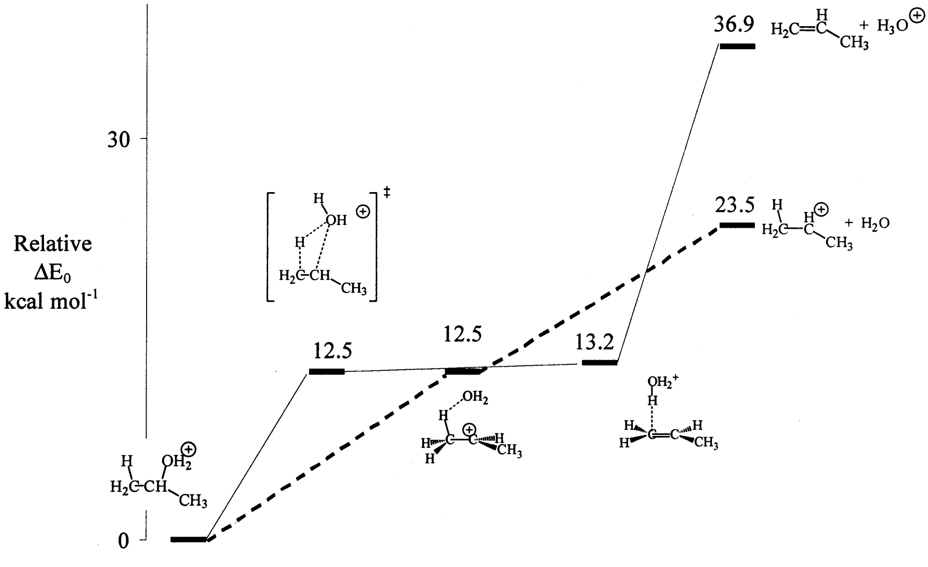

Fig. 4. Schematic drawing showing the energetics for the 1,2-dehydration of protonated isopropanol. The solid line is for reaction (19) and the dashed line is for reaction (20). The calculated relative energies, ΔE_0, are obtained using CBS-QB3 and include zero point energy.

orders of magnitude greater than for neat propanol and the life times, $\tau_{250\ °C} = 3.6$ s, $\tau_{500\ °C} = 4 \times 10^{-5}$ s, are small enough that this reaction should be considered significant in pyrolysis applications.

Significantly, greater stability of the secondary carbocation lowers the enthalpy of reaction (20), which is 9 kcal mol^{-1} more exothermic than the analogous reaction for protonated ethanol.

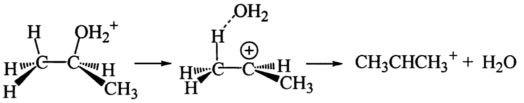

(20)

This reaction ($\Delta_{\mathrm{react}}H_{298} = 25.1$ kcal mol^{-1}) is now thermodynamically favored over reaction (19), $\Delta_{\mathrm{react}}H_{298} = 38.1$ kcal mol^{-1}. Additionally, the water cluster of the carbocation was found to be stable. Calculations of the rate constants for reaction (20) using the energy of reaction, 22.7 kcal mol^{-1}, for E_a and an A factor of 10^{16} s^{-1} yield rate constants that are 15–21 orders of magnitude greater than 1,2-dehydrtion of neat isopropanol. The lifetimes of this reaction, $\tau_{250\ °C} = 3 \times 10^{-7}$ s, $\tau_{500\ °C} = 3 \times 10^{-10}$ s, are small enough to again suggest that this type of reaction may be important in practical systems. Our calculations show that reaction (20) has a rate 5–7 orders of magnitude greater than reaction (19). This is consistent with CID experiments of protonated isopropanol [65]. These studies primarily show the formation of $C_3H_7^+$ ($m/z = 47$) with no H_2O^+ ($m/z = 19$). In summary, secondary alcohols, such as are found in carbohydrates, can easily form carbocations by 1,2-dehydration reactions at relevant temperatures. These cations may be initiators in char forming steps.

3.6. Ethylene glycol

Ethylene glycol serves as a model system for glycol groups in carbohydrates as discussed above. In many respects, the 1,2-dehydration of neat ethylene glycol is similar to dehydration of ethanol.

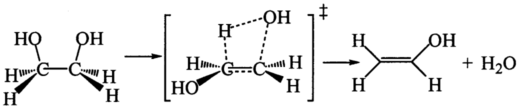

(21)

As Table 1 shows, the energetics are similar, $\Delta_{\mathrm{react}}H_{298} = 7.9$ kcal mol^{-1}, $\Delta E_0 =$ 69.6 kcal mol^{-1} for the transition state, and as Table 2 shows, the transition states structures are similar.

The similarity to ethanol disappears when ethylene glycol is complexed with Li$^+$. This complex is considerably stronger than that formed with ethanol or isopropanol. In its complex with ethylene glycol, Li$^+$ binds to both OH groups. As a result, our calculated binding enthalpy for this complex is 58.4 kcal mol^{-1} (Table 4) while the binding enthalpy of Li$^+$ with ethanol and isopropanol are 38.1 and 39.8 kcal mol^{-1}, respectively. This strong bonding in the ethylene glycol results in a high activation energy for the loss of $H_2O \cdot Li^+$, reaction (22).

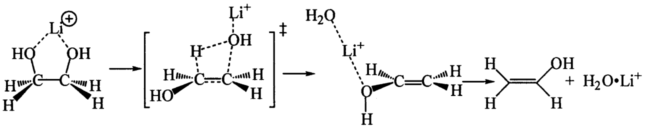

(22)

In the transition state for this reaction, one of the OH groups twists away from the Li^+ and becomes planar with the ethylene group. This effectively breaks one of the Li–O bonds and one would expect that the binding energy of the Li^+ in the transition state to be about that of ethanol or propanol (39 kcal mol^{-1}). This notion is supported by the similarity of the structure for this transition state (Table 2) to that of the transition state for lithiated ethanol. Since there is about 19 kcal mol^{-1} less Li^+ binding energy in the transition state than in the reactant, we would expect the barrier for reaction (22) to be higher than the barrier for lithiated ethanol by about this much. The barrier for lithiated ethanol, reaction (10), is 55.3 kcal mol^{-1} and we expect a barrier of about 74 kcal mol^{-1} for reaction (22). This is in excellent agreement with our calculated value, 74.2 kcal mol^{-1}. This high barrier results in rate constants for reaction (22) that are 1–2 orders of magnitude smaller than the dehydration rate for neat ethylene glycol. Thus, 1,2-dehydration of ethylene glycol is not enhanced by Li^+.

As with ethanol and isopropanol, loss of LiOH from lithiated ethylene glycol, reaction (23), is prohibitively high.

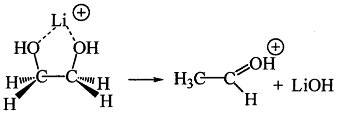

(23)

Note that for this reaction the product cation rearranges to the more stable protonated acetaldehyde. The enthalpy for reaction (23) is 74.5 kcal mol^{-1} and the calculated rate constants are about the same as for dehydration of neat ethylene glycol and thus this reaction is not likely to be important.

Protons, unlike lithium cations facilitate dehydration of ethylene glycol (Fig. 5). With protonated ethylene glycol, the two OH groups do not appear to bind to the proton, and as a result the calculated proton affinity of ethylene glycol (187.1 kcal mol^{-1}) is only slightly higher than the calculated proton affinity of ethanol (182.9 kcal mol^{-1}). Therefore, the calculated relative energy of the transition state is only 27.6 kcal mol^{-1} above the reactant. The structure of the transition state that we obtain for protonated ethylene glycol is similar to that for protonated ethanol and protonated isopropanol as can be seen in Table 2. However, IRC calculations indicate that this transition state connects this transition state to protonated acetaldehyde and water as shown in reaction (24).

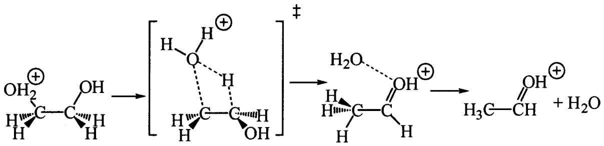

(24)

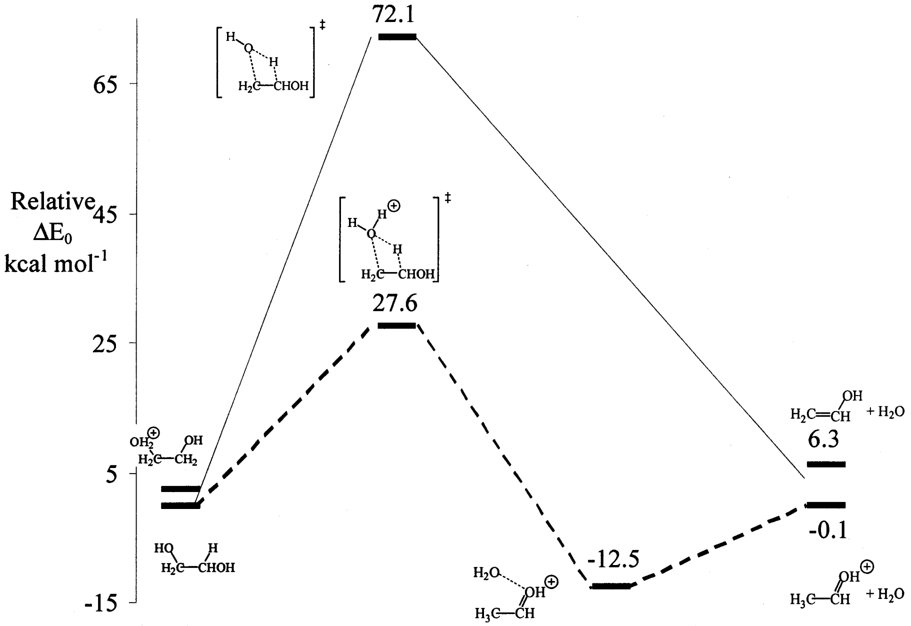

Fig. 5. Schematic diagram of the energetics of the 1,2-dehydration of neat ethylene glycol, solid line, reaction (21), compared with protonated ethylene glycol, dashed line, reaction (24). The calculated relative energies, ΔE_0, are obtained using CBS-QB3 and include zero point energy.

The stability of the resulting oxonium cation accounts for the low enthalpy of this reaction, $\Delta_{\mathrm{react}}H_{298} = 1.6$ kcal mol^{-1}. Since the separated products are at a lower energy than the transition state, we can use the TST methods outlined above to estimate the rate constants for reaction (24). As Table 3 shows, we obtain rate constants that are 13–18 orders of magnitude larger than those for neat ethylene glycol. Lifetimes from these rate constants, $\tau_{250\ ^\circ\mathrm{C}} = 4 \times 10^{-4}$ s, $\tau_{500\ ^\circ\mathrm{C}} = 6 \times 10^{-8}$ s, are small enough that this type of reaction could be important. Oxonium ions such as those formed from reaction (24) could be an important source of cross-linking and char formation in carbohydrate pyrolysis conducted in the presence of acid.

3.7. Implications for carbohydrate pyrolysis

Simple 1,2-dehydrations of all of the neat alcohols studied consistently have barriers of approximately 67–69 kcal mol^{-1}. As Table 1 shows this barrier is independent of size of the alcohol and is the same for glycols groups. Thus, it is reasonable to assume that this barrier is the same for the carbohydrates found in biomass. We have computed the barrier for dehydration in a simple sugar, levoglucosan, to test this hypothesis.

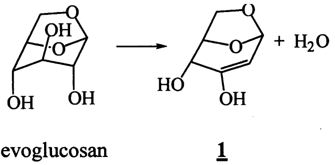

(25)

Since this molecule is a bicyclic species there are a limited number of conformers, which makes the computation easier. It is impractical to conduct CBS-QB3 calculations of this molecule, but the computed barrier for dehydration using B3LYP is possible on a large computer. Our calculations show that the B3LYP barrier, 68 kcal mol^{-1}, is consistent with the calculated barriers for other alcohols, as is shown in Table 1 and it, therefore, seems reasonable to assume that the actual barrier of 1,2-dehydration for levoglucosan and other sugars is 67–69 kcal mol^{-1}.

4. Conclusions

From our investigation of the 1,2-dehydration of alcohols, we can draw several conclusions concerning the importance of these reactions. (i) In general, the addition of alkali metal cations and protons dramatically increases the rates of these reactions. With protonation, the calculated rates are high enough that this process appears likely on a time-scale of typical pyrolysis or torrefaction processes. The increase in rates is primarily due to a decrease in the potential barrier, which is caused by stabilization of transition state. The trend for this effect in terms of decreasing energy of the reaction barrier is neat alcohol $< Na^+ < Li^+ < H^+$. The trend appears to be related to the size of the cation and one would expect that of the two important alkali metals in biomass, K^+ would have a smaller impact than Na^+. (ii) This decrease in the potential barrier becomes larger for a more highly substituted alcohol. This is likely due to greater accommodation of charge by secondary carbons relative to primary carbons. (iii) Greater substitution of the alcohol also leads to the formation of carbocations and oxonium as products. These highly reactive products may serve as cross-linking agents, which can lead to the formation of char during pyrolysis. (iv) Strong metal/glycol bonding slows 1,2-dehydration, because the glycol is stabilized relative to the transition state.

Consider the pyrolysis protonated cellulose. The following shows a potential reaction of protonated cellulose under pyrolysis or torrefaction conditions.

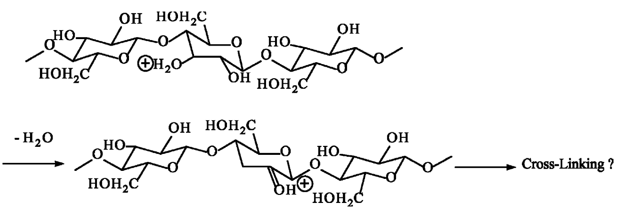

(26)

If our studies of model compounds are applicable, it is reasonable to expect that the first step is fascile under typical conditions. However, this picture may be complicated by the hydrogen bonding found in solid cellulose. The effect of additional hydrogen bonding can and should be investigated in the future. In any event, the reactivity of the resulting oxonium ion makes the subsequent reaction likely.

Acknowledgements

This work was supported by the Philip Morris Corp, grants from the Chemical Physics Program, US Department of Energy (DE-FG02-87ER13695) and a grant from the National Center for Supercomputer Applications (NCSA Grant # CHE-980028n). We would like to gratefully acknowledge the support from Mohammad Hajoligol, Geoffrey Chan and John B. Paine III.

References

[1] J. Bourgois, R. Guyonnet, Wood Sci. Technol. 22 (1988) 143.
[2] J. Bourgois, M.C. Bartholin, R. Guyonnet, Wood Sci. Technol. 23 (1989) 303.
[3] J. Evans, T.A. Milne, Energy Fuels 1 (1987) 123.
[4] D. Lewis, M. Keil, M. Starr, J. Am. Chem. Soc. 96 (1974) 4398.
[5] W. Tsang, Int. J. Chem. Kinet. 8 (1976) 173.
[6] N.I. Butkovskaya, Y. Zhao, D.W. Setser, J. Phys. Chem. 98 (1994) 10779.
[7] A.P. Scott, L. Radom, J. Phys. Chem. 100 (1996) 16502.
[8] T. Shimanouchi, Tables of Molecular Vibrational Frequencies I; NSRDS-NBS 39, National Bureau of Standards, Washington, DC, 1972.
[9] F. Shafizadeh, J. Appl. Polymer Sci. 28 (1975) 153.
[10] G. Dobele, G. Rossinskaja, G. Telysheva, D. Meier, O. Faix, J. Anal. Appl. Pyrolysis 49 (1999) 307.
[11] M.J. Frisch, G.W. Trucks, H.B. Schlegel, G.E. Scuseria, M.A. Robb, J.R. Cheeseman, V.G. Zakrzewski, J.A. Montgomery, Jr, R.E. Stratmann, J.C. Burant, S. Dapprich, J.M. Millam, A.D. Daniels, K.N. Kudin, M.C. Strain, O. Farkas, J. Tomasi, V. Barone, M. Cossi, R. Cammi, B. Mennucci, C. Pomelli, C. Adamo, S. Clifford, J. Ochterski, G.A. Petersson, P.Y. Ayala, Q. Cui, K. Morokuma, P. Salvador, J.J. Dannenberg, D.K. Malick, A.D. Rabuck, K. Raghavachari, J.B. Foresman, J. Cioslowski, J.V. Ortiz, A.G. Baboul, B.B. Stefanov, G. Liu, A. Liashenko, P. Piskorz, I. Komaromi, R. Gomperts, R.L. Martin, D.J. Fox, T. Keith, M.A. Al-Laham, C.Y. Peng, A. Nanayakkara, M. Challacombe, P.M.W. Gill, B. Johnson, W. Chen, M.W. Wong, J.L. Andres, C. Gonzalez, M. Head-Gordon, E.S. Replogle, J.A. Pople, GAUSSIAN 98 (Revision A.1x), Gaussian, Inc, Pittsburgh PA, 2001.
[12] A.D. Becke, Phys. Rev. B 38 (1988) 3098.
[13] C. Lee, W. Yang, R.G. Parr, Phys. Rev. B 37 (1988) 785.
[14] J.A. Montgomery, Jr, M.J. Frisch, J.W. Ochterski, G.A. Petersson, J. Chem. Phys. 110 (1999) 2822.
[15] C. Peng, H.B. Schlegel, J. Chem. Phys. 90 (1989) 2154.
[16] C. Gonzalez, H.B. Schlegel, J. Phys. Chem. 94 (1990) 5523.
[17] E.P. Hunter, S.G. Lias, J. Phys. Chem. Ref. Data 27 (3) (1998) 413.
[18] A.M. Mabel, M.C. Lin, T. Yu, K. Morokuma, J. Phys. Chem. 101 (1997) 3189.
[19] J. Baker, M. Muir, J. Andzelm, J. Chem. Phys. 102 (1995) 2063.
[20] R.V. Stanton, K.M. Merz, Jr, J. Chem. Phys. 100 (1994) 434.
[21] L. Deng, T. Ziegler, Int. J. Quantum Chem. 52 (1994) 731.
[22] J. Baker, J. Andzelm, M. Muir, P.R. Taylor, Chem. Phys. Lett. 237 (1995) 53.

[23] J.L. Durant, Chem. Phys. Lett. 256 (1996) 595.

[24] C.P. Sosa, C. Lee, J. Chem. Phys. 98 (1993) 8004.

[25] J.E. Carpenter, C.P. Sosa, J. Mol. Struct. (Theochem.) 311 (1994) 325.

[26] V. Barone, L. Orlandini, Chem. Phys. Lett. 246 (1995) 45.

[27] P. Nachtigall, K.D. Jordan, A. Smith, H. Jonsson, J. Chem. Phys. 104 (1996) 148.

[28] T. Oie, I.A. Topol, S.K. Burt, J. Phys. Chem. 99 (1995) 905.

[29] K.D. Dobbs, D.A. Dixon, J. Phys. Chem. 98 (1994) 12584.

[30] R.D. Bach, M.N. Glukhovstev, C. Gonzalez, M. Marquez, C.M. Estevez, A.G. Baboul, H.B. Schlegel, J. Phys. Chem. A 101 (1997) 6092.

[31] H. Basch, S. Hoz, J. Phys. Chem. A 101 (1997) 4416.

[32] D. Hodgson, H.-Y. Zhang, M.R. Nimlos, J.T. McKinnon, J. Phys. Chem. 105 (2001) 4316.

[33] C. Peng, P.Y. Ayala, H.B. Schlegel, M.J. Frisch, J. Comp. Chem. 17 (1996) 49.

[34] J. Simons, P. Jorgensen, H. Taylor, J. Ozment, J. Phys. Chem. 87 (1983) 2745.

[35] A. Bannerjee, N. Adams, J. Simons, R. Shepard, J. Phys. Chem. 89 (1985) 52.

[36] C.J. Cerjan, W.H. Miller, J. Chem. Phys. 75 (1981) 2800.

[37] W. Koch, M.C. Holthausen, A Chemist's Guide to Density Functional Theory, second ed., Wiley, New York, 2001.

[38] P.Y. Ayala, H.B. Schlegel, J. Chem. Phys. 108 (1998) 2314.

[39] From $\Delta_f H_{298}$ [$(CH_3)_3COH$] = −74.72 ± 0.21 kcal mol^{-1} ([40]), $\Delta_f H_{298}$ [$(CH_3)_2CCH_2$] = −4.29 ± 0.26 kcal mol^{-1} ([41]), and $\Delta_f H_{298}$ [H_2O] = −57.7978 ± 0.0096 kcal mol^{-1} ([42]).

[40] K.B. Wiberg, S. Hao, J. Org. Chem. 56 (1991) 5108.

[41] E.J. Prosen, F.W. Maron, F.D. Rossini, Heats of combustion, formation, and insomerization of ten C4 hydrocarbons, J. Res. NBS 46 (1951) 106–112.

[42] J.D. Cox, D.D. Wagman, V.A. Medvedev, CODATA Key Values for Thermodynamics, Hemisphere Publishing, New York, 1984, p. 1.

[43] From $\Delta_f H_{298}$ [$(CH_3)_2COHCH(CH_3)_2$] = −85.32 ± 0.14 kcal mol^{-1} ([40]), $\Delta_f H_{298}$ [$(CH_3)_2CCH_2$] = −16.8 ± 0.36 kcal mol^{-1} ([40]), and $\Delta_f H_{298}$ [H_2O] = −57.7978 ± 0.0096 kcal mol^{-1} ([42]).

[44] From $\Delta_f H_{298}$ [CH_3CH_2OH] = −56.23 ± 0.12 kcal mol^{-1} ([45]), $\Delta_f H_{298}$ [CH_2CH_2] = −12.5399 kcal mol^{-1} ([46]), and $\Delta_f H_{298}$ [H_2O] = −57.7978 ± 0.0096 kcal mol^{-1} ([42]).

[45] J.H.S. Green, Chem. Ind. (London) (1960) 1215–1216.

[46] M.W. Chase Jr, J. Phys. Chem. Ref. Data, Monograph 9, (1998) 1–1951.

[47] From $\Delta_f H_{298}$ [$(CH_3)_2CHOH$] = −65.07 ± 0.22 kcal mol^{-1} ([48]), $\Delta_f H_{298}$ [CH_2CHCH_3] = 4.879 kcal mol^{-1} ([49]), and $\Delta_f H_{298}$ [H_2O] = −57.7978 ± 0.0096 kcal mol^{-1} ([42]).

[48] A. Snelson, H.A. Skinner, Trans. Faraday Soc. 57 (1961) 2125–2131.

[49] S. Furuyama, D.M. Golden, S.W. Benson, J. Chem. Thermodyn. 1 (1969) 363–375.

[50] From $\Delta_f H_{298}$ [$HOCH_2CH_2OH$] = −94.26 ± 0.67 kcal mol^{-1} ([51]), $\Delta_f H_{298}$ [CH_2CHOH] = −29.8 ± 2.0 kcal mol^{-1} ([52]), and $\Delta_f H_{298}$ [H_2O] = −57.7978 ± 0.0096 kcal mol^{-1} ([42]).

[51] P. Knauth, R. Sabbah, Struct. Chem. 1 (1990) 43–46.

[52] J.L. Holmes, F.P. Lossing, J. Am. Chem. Soc. 104 (1982) 2648–2649.

[53] From PA(CH_3CH_2OH) = 185.6 kcal mol^{-1} ([17]), $\Delta_f H_{298}$ [CH_3CH_2OH] = −56.23 ± 0.12 kcal mol^{-1} ([45]), $\Delta_f H_{298}$ [CH_2CH_2] = −12.5399 kcal mol^{-1} ([46]), $\Delta_f H_{298}$ [H_2O] = −57.7978 ± 0.0096 kcal mol^{-1} ([42]), PA(H_2O) = 165 kcal mol^{-1} ([17]), $\Delta_f H_{298}$ [H] = 52.103 ± 0.001 kcal mol^{-1} ([42]), IP(H) = 13.59844 eV.

[54] From PA(CH_3CH_2OH) = 185.6 kcal mol^{-1} ([17]), $\Delta_f H_{298}$ [CH_3CH_2OH] = −56.23 ± 0.12 kcal mol^{-1} ([45]), $\Delta_f H_{298}$ [CH_2CH_3] = 28.4 ± 0.5 kcal mol^{-1} ([55]), IP[CH_2CH_3] = 8.117 ± 0.008 eV ([56]), $\Delta_f H_{298}$ [H_2O] = −57.7978 ± 0.0096 kcal mol^{-1} ([42]), $\Delta_f H_{298}$ [H] = 52.103 ± 0.001 kcal mol^{-1} ([42]), IP(H) = 13.59844 eV.

[55] W. Tsang, in: J.A. Martinho Simoes, A. Greenberg, J.F. Liebman (Eds.), Heats of Formation of Organic Free Radicals by Kinetic Methods in Energetics of Organic Free Radicals, Blackie Academic and Professional, London, 1996, pp. 22–58.

[56] B. Ruscic, J. Berkowitz, L.A. Curtiss, J. Chem. Phys. 91 (1989) 114.

[57] From PA[$(CH_3)_2CHOH$] = 189.5 kcal mol^{-1} ([17]), $\Delta_f H_{298}$ [$(CH_3)_2CHOH$] = −65.07 ± 0.22 kcal mol^{-1} ([48]), $\Delta_f H_{298}$ [CH_2CHCH_3] = 4.879 kcal mol^{-1} ([49]), $\Delta_f H_{298}$ [H_2O] = −57.7978 ± 0.0096 kcal

mol^{-1} ([42]), PA(H_2O) = 165 kcal mol^{-1} ([17]), $\Delta_f H_{298}$ [H] = 52.103 ± 0.001 kcal mol^{-1} ([42]), IP(H) = 13.59844 eV.

[58] From PA[$(CH_3)_2CHOH$] = 189.5 kcal mol^{-1} ([17]), $\Delta_f H_{298}$ [$(CH_3)_2CHOH$] = −65.07 ± 0.22 kcal mol^{-1} ([48]), $\Delta_f H_{298}$ [$CH_3CH_2CH_3$] = 22.0 ± 0.5 kcal mol^{-1} ([55]), IP[CH_2CH_3] = 7.37 ± 0.02 eV ([59]), $\Delta_f H_{298}$ [H_2O] = −57.7978 ± 0.0096 kcal mol^{-1} ([42]), $\Delta_f H_{298}$ [H] = 52.103 ± 0.001 kcal mol^{-1} ([42]), IP(H) = 13.59844 eV.

[59] J. Dyke, A. Ellis, N. Jonathan, A. Morris, J. Chem. Soc. Faraday Trans. 2 81 (1985) 1573.

[60] From PA[$HOCH_2CH_2OH$] = 195 kcal mol^{-1} ([17]), $\Delta_f H_{298}$ [$HOCH_2CH_2OH$] = −94.26 ± 0.67 kcal mol^{-1} ([51]), $\Delta_f H_{298}$ [CH_3CHO] = −40.8 ± 0.35 kcal mol^{-1} ([61]), PA[CH_3CHO] = 183.7 kcal mol^{-1} ([17]), $\Delta_f H_{298}$ [H_2O] = −57.7978 ± 0.0096 kcal mol^{-1} ([42]), $\Delta_f H_{298}$ [H] = 52.103 ± 0.001 kcal mol^{-1} ([42]), IP(H) = 13.59844 eV.

[61] K.B. Wiberg, L.S. Crocker, K.M. Morgan, J. Am. Chem. Soc. 113 (1991) 3447–3450.

[62] K.A. Holbrook, M.J. Pilling, S.H. Robertson, Unimoleculra Reactions, second ed., Wiley, New York, 1996.

[63] The structure of $C_2H_5^+$ is actually closer to that of protonated ethylene. That is, the proton is π-bond of ethylene.

[64] D.J. Swanton, D.C.J. Marsden, L. Radom, Org. Mass Spectrom. 21 (1991) 227.

[65] Z. Karpas, G.A. Eiceman, R.G. Ewing, C.S. Harden, Int. J. Mass Spectrom. Ion Processes 133 (1994) 47.

[66] A.G. Harrison, Org. Mass Spectrom. 22 (1987) 637.

[67] J.B. Foresman, Æ. Frisch, Exploring Chemistry with Electronic Structure Methods, second ed., Gaussian Incorporation, Pittsburg, 1995.

[68] A.L.L. East, L. Radom, J. Chem. Phys. 106 (1997) 6655.